Delaminated Graphene at Silicon Carbide Facets: Atomic Scale Imaging and Spectroscopy

Giuseppe Nicotra,[†] Quentin M. Ramasse,[‡] Ioannis Deretzis,[†] Antonino La Magna,[†,*] Corrado Spinella,[†] and Filippo Giannazzo[†]

[†]CNR-IMM, Strada VIII, 5, 95121 Catania, Italy and [‡]SuperSTEM Laboratory, STFC Daresbury Campus, Daresbury WA4 4AD, United Kingdom

ABSTRACT Atomic-resolution structural and spectroscopic characterization techniques (scanning transmission electron microscopy and electron energy loss spectroscopy) are combined with nanoscale electrical measurements (conductive atomic force microscopy) to study at the atomic scale the properties of graphene grown epitaxially through the controlled graphitization of a hexagonal SiC(0001) substrate by high temperature annealing. This growth technique is known to result in a pronounced electron-doping ($\sim 10^{13}$ cm^{-2}) of graphene, which is thought to originate from an interface carbon buffer layer strongly bound to the substrate. The scanning transmission electron microscopy analysis, carried out at an energy below the knock-on threshold for carbon to ensure no damage is imparted to the film by the electron beam, demonstrates that the buffer layer present on the planar SiC(0001) face delaminates from it on the (11$\bar{2}n$) facets of SiC surface steps. In addition, electron energy loss spectroscopy reveals that the delaminated layer has a similar electronic configuration to purely sp^2-hybridized graphene. These observations are used to explain the local increase of the graphene sheet resistance measured around the surface steps by conductive atomic force microscopy, which we suggest is due to significantly lower substrate-induced doping and a resonant scattering mechanism at the step regions. A first-principles-calibrated theoretical model is proposed to explain the structural instability of the buffer layer on the SiC facets and the resulting delamination.

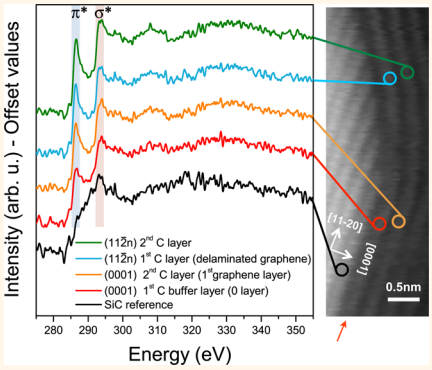

KEYWORDS: epitaxial graphene · SiC · facets · STEM · EELS · buffer layer delamination

Graphene is a planar one-atom-thick layer of sp^2-bonded carbon atoms with remarkable electronic transport properties[1,2] that make it a potential candidate for future electronic applications. In the last years, significant advances have been achieved in the growth of laterally uniform graphene films over large areas, either by thermal decomposition of hexagonal SiC[3] or by chemical vapor deposition on catalytic metals.[4] However, graphene presents specific structural and electronic properties depending on the growth substrate and mechanism, which consequently have an impact on its macroscopic electrical behavior. Thus, many recent investigations (both experimental and theoretical) have focused on understanding the effect of the interaction between graphene and its substrate. Particularly interesting is the case of epitaxial graphene (EG) grown on SiC, where a crucial role is played by the presence of a so-called carbon "buffer layer" or "0 layer" with a $(6\sqrt{3} \times 6\sqrt{3})$R30 hexagonal reconstruction at the interface between graphene and the (0001) face of SiC.[5] Such layer is known to present a certain degree of sp^3 hybridization since it is partially bound to the outmost Si atoms of the SiC(0001) surface. However, a large density of unsaturated Si dangling bonds is left, whose effect is to induce a high n-type doping ($\sim 10^{13}$ cm^{-2}) on the overlying EG.[3,6,7] In the last years, several groups have reported the detachment of the buffer layer from the SiC(0001) basal plane by intercalation with hydrogen,[8] oxygen[9] or metals.[10] The electronic properties of the obtained quasi-free-standing epitaxial graphene (QFEG) have been widely investigated and significant changes in the doping with respect to nonintercalated EG have been observed. In particular, in the case of QFEG obtained on SiC(0001) by H intercalation, a residual p-type doping of $\sim 5 \times 10^{12}$ cm^{-2} is

* Address correspondence to antonino.lamagna@imm.cnr.it.

Received for review September 25, 2012 and accepted March 26, 2013.

Published online March 26, 2013
10.1021/nn305922u

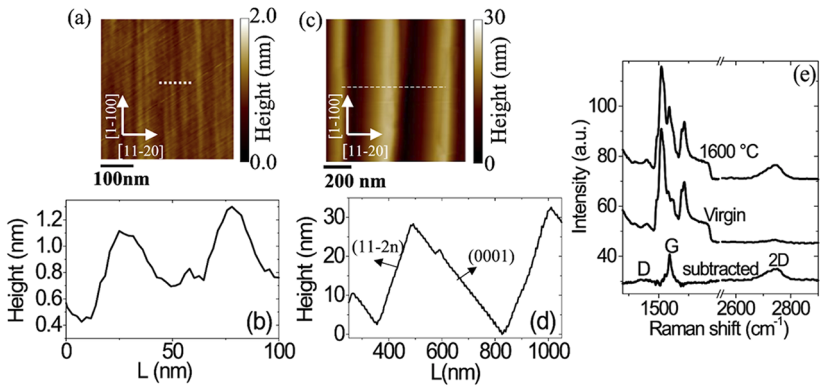

Figure 1. Atomic force microscopy image of the surface morphology (a) and line profile (b) on a virgin 4H-SiC(0001) substrate cut at an angle of 8° with respect to the basal plane along the [11$\bar{2}$0] direction. Surface morphology (c) and line profile (d) of the same substrate after epitaxial graphene growth. (e) Typical micro-Raman spectra on the virgin sample and after EG growth by thermal annealing at 1600 °C. The Raman signal obtained by calculating the difference of the two spectra is also reported. For clarity, the three spectra are offset vertically.

typically observed, compared to the $\sim 10^{13}$ cm^{-2} n-type doping in EG.[11] The origin of the this p-type doping was explained in terms of the polarization induced by the piezoelectric SiC substrate.[12]

Recently, other aspects of the interaction of EG with the substrate have also been investigated, such as an anisotropy of current transport in the directions parallel and orthogonal to the steps.[13−15] Furthermore, a local modification of the conductance in graphene over substrate nanosteps has been demonstrated by nanoscale electrical measurements.[16−18] To explain the additional resistance arising from these steps, calculations have been reported, which took into account the elastic deformation of a graphene membrane over the step profile and a reduction of substrate-induced doping of graphene at the sidewall of the step.[17,18] The latter in particular was predicted to be the main mechanism responsible for the increased resistance. However, a clear atomic-scale identification of the structural and electronic properties at the step region still lacks and would be crucial to definitively explain the observed phenomena.

In this paper, a combination of nanoscale electrical measurements and atomic-resolution structural and spectroscopic characterization techniques was used to study the properties of epitaxial graphene over the steps of off-axis SiC(0001) substrates. The combined analysis provides direct evidence that the buffer layer present on the planar (0001) face of SiC delaminates from the substrate on the (11$\bar{2}n$) facets of the steps, turning into quasi-freestanding graphene. The resulting absence of a buffer layer on the step facets fully explains the observed local increase of the graphene sheet resistance due to lower substrate-induced doping and the effective addition of an extra graphene layer at the step regions. Finally, a first-principles theoretical model is proposed in order to explain the structural instability of the buffer layer on the (11$\bar{2}n$) facets.

RESULTS

Morphological and Electrical Characterization. To ensure that the atomic-scale study is carried out on samples exhibiting the properties characteristic of EG grown on stepped SiC, and in particular the increased resistance over surface steps that has been reported in the literature, a careful morphological and electrical analysis was undertaken as a preparatory step. Panels a and c of Figure 1 show an atomic force microscopy (AFM) analysis of the surface morphology of 4H-SiC(0001) before and after EG growth, respectively. The 4H-SiC substrate exposes both the (0001) basal plane and surfaces with (11$\bar{2}n$) faceting: the virgin SiC samples used here exhibit typical terraces with ∼0.5 nm step height and ∼30−40 nm spacing (see the line profile in Figure.1b), originating from the intentional 8° miscut angle of the substrate chosen to provide a large number of steps for our study. After thermal processing at 1600 °C in 900 mbar Ar atmosphere (see Materials and Methods section for details), the surface morphology changed dramatically, suggesting a surface reconstruction after graphitization with the occurrence of very wide terraces of an average width of 300−400 nm, and high steps (∼20 nm), as shown in the line profile of Figure 1d. Representative micro-Raman spectra were collected on the annealed and virgin 4H-SiC to confirm the success of the epitaxial growth process: these are reported in Figure.1e, along with the Raman signal obtained by subtraction of the pregrowth spectrum from the postannealing spectrum. The occurrence of the characteristic G and 2D peaks[19] in the difference spectrum demonstrates unambiguously the successful formation of few layers of graphene at the surface of the SiC substrate after the thermal process.

The nano- and macro-scale electrical characterization of the grown EG layers is reported in Figure 2, which shows the surface morphology (Figure 2a) and the corresponding current map (Figure 2b) measured by conductive atomic force microscopy (CAFM) on the

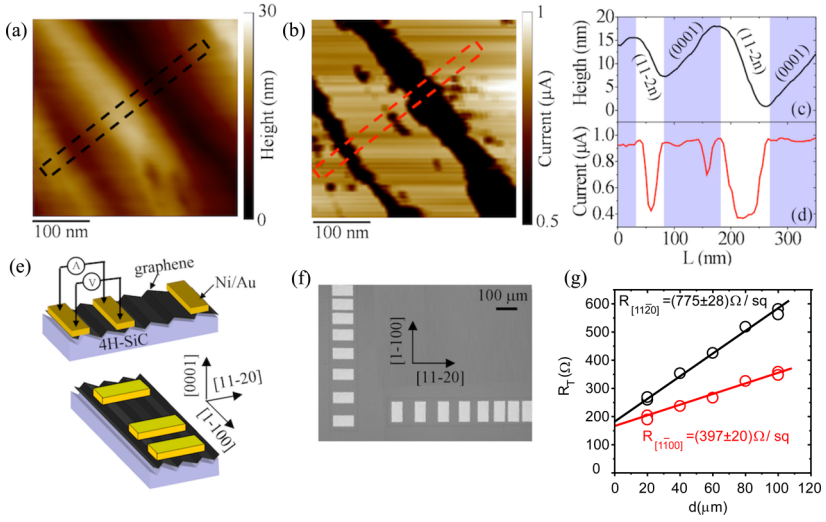

Figure 2. Surface morphology (a) and the corresponding current map (b) measured by conductive atomic force microscopy on the as-grown EG/4H-SiC(0001) sample. Line-profiles of the height (c) and of the current (d) along the indicated directions in the maps. A significant decrease (from 1 to 0.4 μA, *i.e.*, more than a factor of 2) in the local current measured on the (11$\bar{2}n$) facets with respect to the values measured on the (0001) basal plane terraces can be observed. Schematic representations (e) and optical image (f) of transmission line model test patterns fabricated in the direction parallel (*i.e.*, [1$\bar{1}$00]) and orthogonal (*i.e.*, [11$\bar{2}$0]) to substrate steps. (g) Measured resistance R_T between pairs of adjacent pads as a function of the interpad distance. The evaluated sheet resistance in the [11$\bar{2}$0] direction was 775 $\pm$ 28 Ω/sq, almost a factor of 2 higher than the sheet resistance (397 $\pm$ 20 Ω/sq) measured in the [1$\bar{1}$00] direction.

as-grown sample. The current map was obtained by applying a bias to a macroscopic Ohmic contact deposited onto the EG and collecting, point by point during the AFM scan, the value of the electrical current flowing laterally in the EG layers from the nanometric tip to the macroscopic contact. As discussed in the Materials and Methods section, this map contains nanoscale resolution information on the local conductance of EG. The line-profiles of the height and of the current along the indicated directions in the maps are depicted in Figure 2, panels c and d, respectively. It is worth noting the significant decrease from ~1 to ~0.4 μA, *i.e.*, by more than a factor of 2, in the local current measured on the (11$\bar{2}n$) facets compared to the values measured on the (0001) basal plane terraces. This observation indicates a local increase of the EG resistance over these facets.

These local inhomogeneities of the sheet resistance are reflected in the macroscopically measured electronic transport properties of the EG film. Transmission line model (TLM) test patterns, consisting of a set of macroscopic Ohmic contacts at different spacings (from 20 to 100 μm) lithographically defined on a laterally isolated epitaxial graphene strip, were fabricated in order to determine the EG sheet resistance both in the direction parallel (*i.e.*, [1$\bar{1}$00]) and orthogonal (*i.e.*, [11$\bar{2}$0]) to the substrate steps: see the schematics in Figure.2e and an optical micrograph of the resulting pattern in Figure 2f. The measured resistance R between pairs of adjacent pads as a function of the distance between pads shows an asymmetry in the macroscopic current flow along the two directions (Figure 2g). The evaluated sheet resistance in the [11$\bar{2}$0] direction was 775 $\pm$ 28 Ω/sq, almost a factor of 2 higher than the sheet resistance measured in the [1$\bar{1}$00] direction: 397 $\pm$ 20 Ω/sq.

The results of this nano- and macro-scale electrical characterization clearly indicate the expected increase in the sheet resistance of our EG sample over the (11$\bar{2}n$) facets.

Structural Properties at the Atomic Scale. To get a deeper understanding of the origin of this phenomenon, an atomic-resolution structural and spectroscopic investigation of the graphene interface with both the (0001) basal plane and the (11$\bar{2}n$) facets was carried out using an aberration corrected STEM operated at a primary beam energy of 60 keV. The combination of the very high spatial resolution with the ability to work at an operating energy that is below the knock-on threshold for carbon[20] was essential for this work. Indeed, under the experimental conditions used here, atoms in the structure are clearly separated in the high angle annular dark field (HAADF) images, while long electron energy loss spectroscopy (EELS) acquisitions are possible without damaging the EG structure (see Materials and Methods section).

Figure 3a–d shows atomic resolution HAADF-STEM images of the 4H-SiC/EG interface acquired on a sample cross-sectioned perpendicularly to the [1$\bar{1}$00] direction (see Materials and Methods section for details of the sample preparation). The (0001) basal plane and the (11$\bar{2}n$) facets form an angle φ, as illustrated in the inset of Figure 3a. The value of this angle ranges from 27° to 34°: the histogram of Figure.3b shows the typical distribution in angular value, obtained from measurements on a set of 10 different steps imaged by STEM.

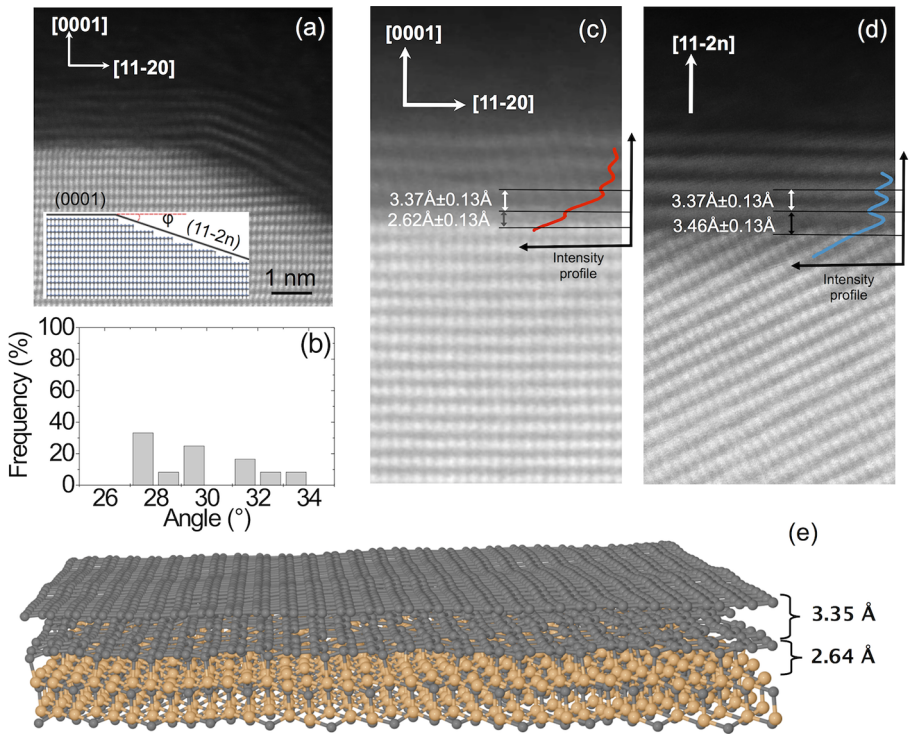

Figure 3. (a) HAADF atomic resolution STEM image of a step facet in the EG/4H-SiC sample cross sectioned along the [11$\bar{2}$0] direction, acquired at a 60 keV primary beam energy to prevent beam-induced damage to the sample. Four carbon layers are resolved at the atomic-scale. (Inset) Schematic of the epitaxial graphene grown on a (11$\bar{2}$*n*) SiC nanofacet structure, showing the angle φ between the (0001) plane and the (11$\bar{2}$*n*) facet. (b) Statistical distribution of the angle φ on the analyzed specimens. (c) Intensity profiles orthogonal to the (0001) surfaces. (d) Intensity profiles orthogonal to the (11$\bar{2}$*n*) surfaces. The carbon buffer layer, visible on the planar (0001) surface, becomes quasi-freestanding graphene on the (11$\bar{2}$*n*) facet. (e) *Ab initio* simulations show the equilibrium average distance between the center of the Si−C dimer on the (0001) planar surface and the buffer layer, and between the buffer layer and the first graphene layer. Si atoms are represented as large brown spheres, while C atoms as smaller gray-colored spheres. The micrographs were acquired in different regions far away from the SiC step 'elbow', so that the interlayer distances would be unaffected by the distortion.

The graphene layers are clearly resolved at the atomic scale, allowing for a precise measurement of the distances between the different carbon layers and the planar (0001) and (11$\bar{2}$*n*) SiC surfaces, as shown in the linescans of Figure 3c,d. The measured distance between the (0001) surface and the first carbon layer was 2.62 $\pm$ 0.13 Å, indicating a very strong bonding of this layer to the substrate: see Figure 3c. By contrast, the distance between the (11$\bar{2}$*n*) surfaces and the first C layer above these facets was found to be 3.46 $\pm$ 0.13 Å, which is even larger than the 3.37 $\pm$ 0.13 Å value of the graphitic interlayer distance (see Figure 3d). It should be noted that the bulk SiC lattice was used as an internal calibration for these measurements. This clear morphological difference provided a first indication that the first C layer in the stack has a different nature depending on the orientation of the underlying substrate: it can be identified with the buffer-layer on the planar (0001) surface of Figure 3a, whereas it appears to delaminate from the (11$\bar{2}$*n*) surface.

We note here that the experimental results were in extremely good agreement with *ab initio* calculations (see Materials and Methods section) of the equilibrium average distances between the center of the Si−C dimer on the (0001) planar surface and the buffer layer, and between the buffer layer and the overlying graphene layer. A model of the stable, fully relaxed structure predicted by the density functional theory (DFT) is depicted on Figure 3e, with interlayer distances of 2.64 and 3.35 Å for the SiC dimer/buffer layer and buffer layer/first graphene layer, respectively.

Electronic Structure. To strengthen this purely structural evidence, the electronic structure of the individual C layers was probed through atomic-scale EELS imaging. Figure 4 shows example spectra extracted from the 2-dimensional spectrum image of a surface step at the positions indicated on the simultaneously acquired HAADF image. The individual C layers are clearly visible in the image, while the distance between the first C layer and the substrate ostensibly increases over the transition from a flat (0001) surface to a (11$\bar{2}$*n*) facet, as previously described. Importantly, marked differences appear in the fine structure of the C K edge depending on the layer for which the spectrum was acquired. The K edge of carbon typically comprises a sharp peak at 285 eV when 1s to π^* electronic transitions are present. The intensity of this peak is therefore related to π bonding, and in the experimental

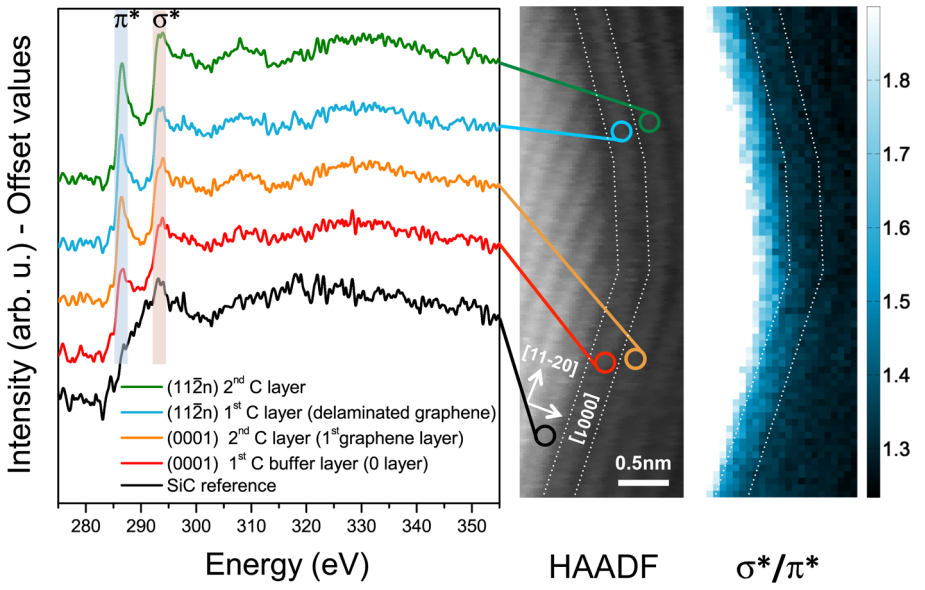

Figure 4. EELS spectra (left) extracted from a 2D spectrum image acquired on a SiC step. The simultaneously acquired HAADF STEM image is shown in the center and reveals a faceted step in the annealed 4H-SiC sample cross-sectioned along the [11$\bar{2}$0] direction. (Right) σ^*/π^* ratio map calculated by integrating the shaded areas indicated on the spectra, left. This map shows that the buffer layer in the region immediately above the (0001) surface (a dotted line indicates the position of the SiC surface as a guide to the eye) exhibits a stronger σ^*/π^* ratio than the other graphene layers, in particular in the region above the (11$\bar{2}n$) surface.

geometry used here (where flat EG layers are being observed by STEM in cross section), it can be directly associated with the presence of sp^2 hybridization, as it is expected for graphene. For instance, the peak is quite prominent on the second C layer of the planar (0001) surface and on the rightmost regions of the spectrum image, corresponding to the outer EG layers. However, the π^* peak intensity drops significantly at the first C layer of the planar (0001) surface, that is, at the buffer layer. The reduction of the amount of π^* bonding at the buffer layer is accompanied by a simultaneous increase of σ^* bonding, seen through the increasing strength of the second peak in the EELS K edge at ~295 eV, which indicates the presence of sp^3 hybridization. The fine structure of the EELS spectra obtained on the first C layer above the planar (0001) surface provides a direct atomic-scale evidence of the validity of the generally agreed model of a partially sp^3-hybridized buffer layer due to the strong bonding with the outmost Si atoms of the SiC substrate.[5]

By contrast, when following the first C layer from the (0001) surface to the (11$\bar{2}n$) facet, the π^* peak intensity at 285 eV increases to a value comparable to what is measured on the outer graphene layers. This suggests the absence of any sp^3-hybridization in the first layer above the SiC(11$\bar{2}n$) facet; hence, it can no longer be described as a buffer layer but as a pure graphene-like layer on top of the surface facets.

These results are better visualized by generating a σ^*/π^* ratio map from the EELS spectrum image, using the areas shaded on the graph that correspond to either the π^* or the σ^* peaks for the signal integration (Figure 4, right). Although the ratio map on its own is not to be considered as a quantitative measurement of the sp^3/sp^2 bond content, the intensity along the layer immediately above the SiC surface (indicated by a dashed line as a guide to the eye) is higher along the (0001) section of the surface: more σ^* transitions indicate the presence of sp^3 bonding in this specific area, but nowhere else, in particular not above the (11$\bar{2}n$) section of the SiC surface. We can therefore conclude that the first C layer in EG can only be described as a partially sp^3-hybridized "buffer layer" when it is strongly bonded to the underlying Si atoms of the SiC(0001) surface. No such buffer behavior is observed on the (11$\bar{2}n$) facets of our 8° off-axis SiC, where the first C layer behaves simply as quasi-freestanding graphene. Analogue data sets were acquired on more than 10 stepped edges, resulting in very similar spectra. We therefore exclude, within the experimental accuracy, any influence of effects such as mistilt or roughness.

The repercussions for the electronic transport properties of the EG/SiC system of what could be described as a buffer layer 'instability' over the SiC facets could be significant. According to the structural model suggested from the microscopy results, two intrinsic scattering mechanisms should be triggered at the (11$\bar{2}n$) facets: the first one is related to the presence of a monolayer/bilayer graphene junction (or more generally with a *i*-layer/(*i* + 1)-layer junction).[17,21] The second has to do with the close proximity of two graphene areas with a significant difference in their doping levels, considering that the high electron-doping of

the (0001) plane is inherent to the presence of the buffer layer.[22]

Theoretical Modeling. To better understand the bonding behavior of epitaxial graphene on the (11$\bar{2}$*n*) facets of 4H-SiC, we constructed a simple model based on energetic considerations obtained from DFT calculations. We adopted the formulation of ref 23 and decomposed the interface energy E_{int} between graphene and the SiC substrate into three constituent components:

$$E_{int} = E_b + E_{str} + E_{def} \quad (1)$$

where E_b is the binding energy defined as:

$$E_b = E_{gr/SiC} - (E_{gr} + E_{SiC}) \quad (2)$$

at the "frozen" positions of the relaxed configuration, E_{str} is the tensile or compressive strain energy for the graphene sheet and E_{def} is the energy due to a perpendicular deformation with respect to the ideal planar geometry of the honeycomb lattice. Out of the three components of eq 1, E_b tends to lower E_{int}, whereas the other two tend to increase it. Within this context, a graphene structure is stable only if $E_{int} < 0$. A direct estimation of E_{int} for the various (11$\bar{2}$*n*) planes is prohibiting within the DFT due to extremely long translation symmetries and the periodicity imposed by the Bloch theorem. However, calculations are possible for the lower and higher limit of these planes, *i.e.*, when $n = 0$ and $n \rightarrow \infty$. In the latter case, $\lim_{n\rightarrow\infty}(11\bar{2}n) =$ (0001) and the problem reduces to the well-studied graphene/SiC(0001) interface. In this case, a $(6\sqrt{3} \times 6\sqrt{3})$R30° reconstructed buffer layer forms on top of the SiC(0001) surface, for which $E_b = -0.35$ eV and $E_{def} = 0.246$ eV per carbon atom, respectively.[23] Note that the strain term here is negligible due to the commensurability of the two parts of the interface. On the contrary, the nonzero value of E_{def} shows that the graphene buffer layer has an important percentage of sp^3-type bonds. On the basis of the same exchange/correlation scheme, we performed DFT calculations for the case when $n = 0$ [*i.e.*, for the graphene/SiC(11$\bar{2}$0) heterosystem, see Supporting Information for details]. We found that in the most stable interfacial configuration, graphene detaches from the substrate and no buffer layer is formed. This structural detachment translates in energetic terms as $E_b = -0.01$ eV, whereas planarity and commensurability minimize E_{def} and E_{str}. Considering that the (0001) and (11$\bar{2}$0) planes form right angles and assuming that the binding energy changes linearly between them, we define the binding energy loss E_φ per angle degree as:

$$E_{\varphi[(0001)\rightarrow(11\,-\,20)]} = (E_{b(11\bar{2}0)} - E_{b(0001)})/90 = 0.00378\text{eV/degree} \quad (3)$$

where $\varphi = \tan^{-1}(\text{length}_{(11\bar{2}0)}/\text{length}_{(0001)})$ at the facet region. In order for the (0001) buffer layer to maintain its stability on an arbitrary (11$\bar{2}$*n*) plane, the condition:

$$|E_{b(0001)}| - \varphi \cdot E_\varphi > E_{def(0001)} + E_{str(0001)} \quad (4)$$

has to be satisfied. This takes place for angles $\varphi \leq 27.51°$. This value could be subject to a further decrease, as recent experiments[24,25] have shown the presence of local strain for graphene on the surface steps of SiC(0001). On the other hand, the possibility that the critical value φ becomes smaller due an increase of the deformation energy on the (11$\bar{2}$*n*) plane with respect to the (0001) case is rather improbable, given that the gradual increase in the concentration of the carbon atoms at the facet region [(0001): 0%, (11$\bar{2}$0): 50%] should result in a local contraction of the deformation of the buffer layer.[26,27] In its present form, this model gives a first-order explanation of the statistical absence of a buffer layer seen from the HAADF images of our 8°-off 4H-SiC sample, where the measured φ angles oscillate between 27 and 34°. As a final remark, we theoretically argue that the formation and stability of a buffer layer on top of the (11$\bar{2}$*n*) steps of an off-axis SiC substrate is inherently correlated with the (0001)/(11$\bar{2}$*n*) angle, as shown above.

CONCLUSIONS AND DISCUSSION

In summary, we presented an atomic-scale study of faceted graphene/SiC interfaces focusing specifically on the structure and properties of the first carbon layer epitaxially grown over the SiC substrate. Conductive atomic force microscopy was used to confirm a local increase of the graphene sheet resistance over SiC facets. By observing this structure at atomic resolution in an aberration-corrected electron microscope, we were able to show that the so-called buffer layer present at the EG/SiC(0001) interface delaminates from the substrate on the (11$\bar{2}$*n*) facets of 8° off-axis SiC, acquiring quasi-freestanding characteristics. Atomic resolution Z-contrast images revealed a striking increase in the distance between the substrate and the first carbon layer over the (11$\bar{2}$*n*) steps with respect to the distance between the (0001) surface and the buffer layer. Furthermore, fine structure analysis of EELS spectrum images provided direct evidence, at the atomic scale, that the sp^3 character of the buffer layer disappears over the SiC facets, whereas the carbon K edge recovers graphene-like characteristics. This finding is of crucial importance for the local modification of the electrical characteristics of EG on SiC steps, since it should trigger intrinsic scattering mechanisms that are related with areas of unequal doping and unequal number of graphene layers. We note that, recently, Hicks *et al.*[28] have demonstrated *via* angle-resolved photoemission spectroscopy and low-energy electron diffraction that EG grown on particular SiC facets looses the $(6\sqrt{3} \times 6\sqrt{3})$R30 periodicity and acquires a mild p-type doping. We consider such results compatible with the detachment effect discussed here. The presence of facets should therefore locally alter the

structural and electrical properties of EG grown on off-axis SiC(0001). This aspect could be of significant impact for the comprehension of the intrinsic mechanisms that rule device operation in EG systems.[29]

MATERIALS AND METHODS

Graphene Growth. Experiments were carried out on 4H-SiC (0001) substrates with an 8° off-axis miscut angle in the [11$\bar{2}$0] direction, over which a low-doped (10^{14} cm^{-2}) micrometer thick SiC epitaxial layer was grown. Graphene growth was performed using a Centrotherm Activator150 furnace. The annealing was carried out at a temperature of 1600 °C in inert gas (Ar) atmosphere at atmospheric pressure (900 mbar), in order to minimize the rate of Si sublimation from the SiC surface, thus obtaining high quality epitaxial graphene growth.[3,30]

Micro-Raman Measurements. Raman analysis was performed using a Horiba-Jobin Yvon spectrometer in the backscattering configuration using a 633 nm laser source and a 100× objective magnification, yielding a spot size of 1 μm.

TEM Specimen Preparation. Mechanical thinning followed by very low energy ion milling (3 keV) was performed just from the SiC bulk side in order to cover graphene by the shadow of the bulk and avoid direct ion hitting.

STEM Characterization. This study was performed using a Nion UltraSTEM100 dedicated aberration-corrected scanning transmission electron microscope. The microscope was operated in the so-called "gentle STEM" conditions at 60 keV primary beam energy,[31] with the probe-forming optics configured to provide a beam convergence half-angle of 30 mrad for an estimated probe size of 1.1 Å. The microscope is equipped with a cold field emission gun with a native energy of 0.35 eV. The high angle annular dark field detector inner and outer radii were calibrated at 85 and 190 mrad, respectively. The energy loss spectrometer was set up with a collection angle of 36 mrad and the energy dispersion was chosen to detect the C K and Si $L_{2,3}$ EELS edges simultaneously. In these conditions, the energy resolution for the experiments is limited by the detector point-spread function and estimated at 0.6 eV from the full width at half-maximum of the zero-loss peak. All reported EELS spectra are raw data, background subtracted using a power law fitted over a 50 eV immediately before the C K edge. The σ^*/π^* ratio map of Figure 4 was obtained from the denoised spectrum image using PCA, background subtracted using a power law fitted over 50 eV immediately before the C K edge, while the σ^* and π^* intensities were integrated over the windows indicated on the left panel of the figure .

Conductive Atomic Force Microscopy. AFM measurements were carried out with a DI3100 atomic force microscope (AFM) supplied by Veeco with Nanoscope V electronics. Pt/Ir coated highly doped Si tips (tip apex curvature radius $r_{tip} \approx 20$ nm) were used. Local conductance maps were obtained by measuring the current flowing laterally in EG between the nanometric tip scanning 1 μm × 1 μm areas and a macroscopic Ohmic contact (made by Ni/Au bilayers). During the scan, a bias was applied to the macroscopic contact and the current was measured by a current amplifier connected to the tip. The measured resistance R is the sum of different contributions, *i.e.*, the contact resistance between the tip and EG (R_{c_tip}), the spreading resistance (R_{spr}) encountered by the current to spread from the tip to the graphene, the series resistance (R_{series}) and the macroscopic contact resistance (R_{c_macro}). Both the R_{c_tip} and R_{spr} contributions contain local information on EG electrical properties, with R_{spr} related to local graphene resistance. To evaluate the weight of the two terms, *i.e.*, to understand whether the contrast in the CAFM maps between the (11$\bar{2}n$) facets and the (0001) basal plane is mainly due to lateral variation of R_{c_tip} or to changes in EG resistance, CAFM measurements in a region very close to the macroscopic contact were performed, as reported in the Supporting Information. Moving the tip from the contact region into EG, a sudden increase of the resistance associated to the R_{c_tip} contribution was observed. Interestingly, the obtained R_{c_tip} values were comparable for the (0001) and (11$\bar{2}n$) faces. Moving further from the contact, a higher slope of the resistance increase as a function of the distance from the contact was found at the (11$\bar{2}n$) facet compared to the basal plane. These observations indicated that the current variations in the CAFM maps on the (11$\bar{2}n$) and (0001) faces must be associated primarily to local variations of the graphene resistance.

First-Principles Calculations. Calculations were based on the density functional theory using the SIESTA code.[32] For the structural information appearing in the third paragraph, we used the computational scheme of ref 22. For graphene on the (11$\bar{2}$0) surface of a 4H-SiC substrate, we used the Perdew-Burke-Ernzerhof implementation[33] of the generalized gradient approximation. We constructed rectangular and commensurate supercells containing single-layer graphene and the SiC substrate according to the following scheme: the graphene sheet was defined by a rectangle with $N_a = 16$ dimer lines parallel to the [1$\bar{1}$00] direction and $N_z = 10$ zigzag chains parallel to the [0001] direction. Underneath, the unreconstructed SiC substrate consisted of five (4 × 2) SiC(11$\bar{2}$0) layers. We used a double-ζ plus polarization basis-set for Si and C, while single-ζ orbitals were used for the hydrogen atoms that passivated the lower termination of the slab. The electronic contribution of the ionic cores was statically included by means of standard norm-conserving pseudopotentials.[34] We used a (2 × 2 × 1) Monkhorst-Pack grid for the sampling of the rectangular Brillouin zone, while real-space integrals were evaluated on a mesh with a cutoff energy of 280 Ry. Atomic and supercell relaxation was imposed until forces were less than 0.04 eV/Å.

Conflict of Interest: The authors declare no competing financial interest.

Acknowledgment. The authors would like to thank E. Rimini, F. Roccaforte and C. Bongiorno for fruitful discussions, O. L. Krivanek and N. Dellby from Nion Co. for giving us the opportunity to interact with the SuperSTEM Laboratory, P. Schmid and W. Lerch from Centrotherm (Blaubeuren, Germany) for the collaboration in epitaxial graphene growth, S. Pannitteri and S. Di Franco from CNR-IMM (Catania, Italy) for their help in TEM sample preparation and device processing, and N. Piluso from CNR-IMM (Catania, Italy) for Raman measurements. F.G., I.D., and A.L. would like to acknowledge the European Science Foundation (ESF) under the EUROCORES Program EuroGRAPHENE CRP GRAPHIC-RF for partial financial support. G.N. and C.S. acknowledge the Italian Ministry of Education and Research (MIUR) under project Beyond-Nano (PON a3_00363). The SuperSTEM Laboratory is supported by the U.K. Engineering and Physical Sciences Research Council (EPSRC). This work had been strongly desired by the late Vito Raineri. We dedicate it to his memory.

Supporting Information Available: Electrical characterization, CAFM measurements, STEM visualization, EELS spectra, and theoretical calculations. This material is available free of charge *via* the Internet at http://pubs.acs.org.

REFERENCES AND NOTES

1. Geim, A. K.; Novoselov, K. S. The Rise of Graphene. *Nat. Mater.* **2007**, *6*, 183–191.
2. Mayorov, A. S.; Gorbachev, R. V.; Morozov, S. V.; Britnell, L.; Jalil, R.; Ponomarenko, L. A.; Blake, P.; Novoselov, K. S.; Watanabe, K. Taniguchi *et al.* Micrometer-Scale Ballistic Transport in Encapsulated Graphene at Room Temperature. *Nano Lett.* **2011**, *11*, 2396–2399.
3. Emtsev, K. V.; Bostwick, A.; Horn, K.; Jobst, J.; Kellogg, G. L.; Ley, L.; McChesney, J. L.; Ohta, T.; Reshanov, S. A.; Rohrl, J.; et al. Towards Wafer-Size Graphene Layers by Atmospheric Pressure Graphitization of Silicon Carbide. *Nat. Mater.* **2009**, *8*, 203–207.
4. Li, X.; Cai, W.; An, J.; Kim, S.; Nah, J.; Yang, D.; Piner, R.; Velamakanni, A.; Jung, I.; Tutuc, E.; et al. Large-Area

Synthesis of High-Quality and Uniform Graphene Films on Copper Foils. *Science* **2009**, *324*, 1312–1314.
5. Varchon, F.; Feng, R.; Hass, J.; Li, X.; Nguyen, B. N.; Naud, C.; Mallet, P.; Veuillen, J. Y.; Berger, C.; Conrad, E. H.; et al. Electronic Structure of Epitaxial Graphene Layers on SiC: Effect of the Substrate. *Phys. Rev. Lett.* **2007**, *99*, 126805.
6. Sonde, S.; Giannazzo, F.; Raineri, V.; Yakimova, R.; Huntzinger, J.-R.; Tiberj, A.; Camassel, J. Electrical Properties of the Graphene/4H-SiC (0001) Interface Probed by Scanning Current Spectroscopy. *Phys. Rev. B* **2009**, *80*, 241406.
7. Sonde, S.; Giannazzo, F.; Vecchio, C.; Yakimova, R.; Rimini, E.; Raineri, V. Role of Graphene/Substrate Interface on the Local Transport Properties of the Two-Dimensional Electron Gas. *Appl. Phys. Lett.* **2010**, *97*, 132101.
8. Riedl, C.; Coletti, C.; Iwasaki, T.; Zakharov, A.; Starke, U. Quasi-Free-Standing Epitaxial Graphene on SiC Obtained by Hydrogen Intercalation. *Phys. Rev. Lett.* **2009**, *103*, 246804.
9. Oliveira, M. H., Jr.; Schumann, T.; Fromm, F.; Koch, R.; Ostler, M.; Ramsteiner, M.; Seyller, T.; Lopes, J. M. J.; Riechert, H. Formation of High-Quality Quasi-Free-Standing Bilayer Graphene on SiC(0001) by Oxygen Intercalation Upon Annealing in Air. *Carbon* **2013**, *52*, 83–89.
10. Virojanadara, C.; Watcharinyanon, S.; Zakharov, A. A.; Johansson, L. I. Epitaxial Graphene on 6H-SiC and Li Intercalation. *Phys. Rev. B* **2010**, *82*, 205402.
11. Speck, F.; Jobst, J.; Fromm, F.; Ostler, M.; Waldmann, D.; Hundhausen, M.; Weber, H.; Seyller, T. The Quasi-Free-Standing Nature of Graphene on H-saturated SiC(0001). *Appl. Phys. Lett.* **2011**, *99*, 122106.
12. Ristein, J.; Mammadov, S.; Seyller, T. Origin of Doping in Quasi-Free-Standing Graphene on Silicon Carbide. *Phys. Rev. Lett.* **2012**, *108*, 246104.
13. Yakes, M. K.; Gunlycke, D.; Tedesco, J. L.; Campbell, P. M.; Myers-Ward, R. L.; Eddy, C. R., Jr.; Gaskill, D. K.; Sheehan, P. E.; Laracuente, A. R. Conductance Anisotropy in Epitaxial Graphene Sheets Generated by Substrate Interactions. *Nano Lett.* **2010**, *10*, 1559–1562.
14. Odaka, S.; Miyazaki, H.; Li, S.-L.; Kanda, A.; Morita, K.; Tanaka, S.; Miyata, Y.; Kataura, H.; Tsukagoshi, K.; Aoyagi, Y. Anisotropic Transport in Graphene on SiC Substrate with Periodic Nanofacets. *Appl. Phys. Lett.* **2010**, *96*, 062111.
15. Schumann, T.; Friedland, K.-J.; Oliveira, M. H., Jr.; Tahraoui, A.; Lopes, J. M. J.; Riechert, H. Anisotropic Quantum Hall Effect in Epitaxial Graphene on Stepped SiC Surfaces. *Phys. Rev. B* **2012**, *85*, 235402.
16. Kuramochi, H.; Odaka, S.; Morita, K.; Tanaka, S.; Miyazaki, H.; Lee, M. V.; Li, S. L.; Hiura, H.; Tsukagoshi, K. Role of Atomic Terraces and Steps in the Electron Transport Properties of Epitaxial Graphene Grown on SiC. *AIP Adv.* **2012**, *2*, 012115.
17. Ji, S.-H.; Hannon, J. B.; Tromp, R. M.; Perebeinos, V.; Tersoff, J.; Ross, F. M. Atomic-Scale Transport in Epitaxial Graphene. *Nat. Mater.* **2011**, *11*, 114–119.
18. Low, T.; Perebeinos, V.; Tersoff, J.; Avouris, Ph. Deformation and Scattering in Graphene over Substrate Steps. *Phys. Rev. Lett.* **2012**, *108*, 096601.
19. Lee, D.; Riedl, C.; Krauss, B.; von Klitzing, K.; Starke, U.; Smet, J. H. Raman Spectra of Epitaxial Graphene on SiC and of Epitaxial Graphene Transferred to SiO_2. *Nano Lett.* **2008**, *8*, 4320–4325.
20. Krivanek, O. L.; Chisholm, M. F.; Nicolosi, V.; Pennycook, T. J.; Corbin, G. J.; Dellby, N.; Murfitt, M. F.; Own, C. S.; Szilagy, Z. S.; Oxley, M. P.; et al. Atom-By-Atom Structural and Chemical Analysis by Annular Dark-Field Electron Microscopy. *Nature* **2010**, *464*, 571–574.
21. Giannazzo, F.; Deretzis, I.; La Magna, A.; Roccaforte, F.; Yakimova, R. Electronic Transport at Monolayer-Bilayer Junctions in Epitaxial Graphene on SiC. *Phys. Rev. B* **2012**, *86*, 235422.
22. Deretzis, I.; La Magna, A. Role of Covalent and Metallic Intercalation on the Electronic Properties of Epitaxial Graphene on SiC(0001). *Phys. Rev. B* **2011**, *84*, 235426.
23. Sclauzero, G.; Pasquarello, A. Carbon Rehybridization at the Graphene/SiC(0001) Interface: Effect on Stability and Atomic-Scale Corrugation. *Phys. Rev. B* **2012**, *85*, 161405.
24. Nakatsuji, K.; Yoshimura, T.; Komori, F.; Morita, K.; Tanaka, S. Uniaxial Deformation of Graphene Dirac Cone on a Vicinal SiC Substrate. *Phys. Rev. B* **2012**, *85*, 195416.
25. Grodecki, K.; Bozek, R.; Strupinski, W.; Wysmolek, A.; Stepniewski, R.; Baranowski, J. M. Micro-Raman Spectroscopy of Graphene Grown on Stepped 4H-SiC (0001) Surface. *Appl. Phys. Lett.* **2012**, *100*, 261604.
26. Pankratov, O.; Hensel, S.; Bockstedte, M. Electron Spectrum of Epitaxial Graphene Monolayers. *Phys. Rev. B* **2010**, *82*, 121416.
27. Deretzis, I.; La Magna, A. A Density Functional Theory Study of Epitaxial Graphene on the (3×3)-Reconstructed C-Face of SiC. *Appl. Phys. Lett.* **2013**, *102*, 093101.
28. Hicks, J.; Tejeda, A.; Taleb-Ibrahimi, A.; Nevius, M. S.; Wang, F.; Shepperd, K.; Palmer, J.; Bertran, F.; Le Fèvre, P.; Kunc, J.; et al. A Wide Bandgap Metal–Semiconductor–Metal Nanostructure Made Entirely from Graphene. *Nat. Phys.* **2013**, *9*, 49–54.
29. Hertel, S.; Waldmann, D.; Jobst, J.; Albert, A.; Albrecht, M.; Reshanov, S.; Schöner, A.; Krieger, M.; Weber, H. B. Tailoring The Graphene/Silicon Carbide Interface for Monolithic Wafer-Scale Electronics. *Nat. Commun.* **2012**, *3*, 957.
30. Virojanadara, C.; Syvajarvi, M.; Yakimova, R.; Johansson, L. I.; Zakharov, A. A.; Balasubramanian, T. Homogeneous Large-Area Graphene Layer Growth on 6HSiC(0001). *Phys. Rev. B* **2008**, *78*, 245403.
31. Krivanek, O. L.; Corbin, G. J.; Dellby, N.; Elston, B. F.; Keyse, R. J.; Murfitt, M. F.; Own, C. S.; Szilagyi, Z. S.; Woodruff, J. W. An Electron Microscope for the Aberration-Corrected Era. *Ultramicroscopy* **2008**, *108*, 179.
32. Soler, J. M.; Artacho, E.; Gale, J. D.; García, A.; Junquera, J.; Ordejón, P.; Sánchez-Portal, D. The SIESTA Method for *ab Initio* Order-N Materials Simulation. *J. Phys.: Condens. Matter* **2002**, *14*, 2745.
33. Perdew, J. P.; Burke, K.; Ernzerhof, M. Generalized Gradient Approximation Made Simple. *Phys. Rev. Lett.* **1996**, *77*, 3865.
34. Troullier, N.; Martins, J. L. Efficient Pseudopotentials for Plane-Wave Calculations. *Phys. Rev. B* **1991**, *43*, 1993.